Use of an Areal Distribution of Mixing Intensity to Describe Blending of Non-Newtonian Fluids in a Kenics KM Static Mixer Using PLIF

F. Alberini, M. J. H. Simmons, and A. Ingram
School of Chemical Engineering, University of Birmingham, Birmingham B15 2TT, U.K.

E. H. Stitt
Johnson Matthey Technology Centre, Billingham TS23 1LB, U.K.

DOI 10.1002/aic.14237
Published online October 4, 2013 in Wiley Online Library (wileyonlinelibrary.com)

The performance of KM static mixers has been assessed for the blending of Newtonian and time-independent non-Newtonian fluids using planar laser induced fluorescence (PLIF). A stream of dye is injected at the mixer inlet and the distribution of dye at the mixer outlet is analyzed from images obtained across the pipe cross section. The effect of number of mixing elements, fluid rheology, and apparent viscosity ratio for two-fluid blending have been investigated at constant mixture superficial velocity of 0.3 m s^{-1}*. Aqueous solutions of glycerol and Carbopol 940 are used as the working fluids, the latter possessing Herschel–Bulkley rheology. The PLIF images have been analyzed to determine log variance and maximum striation thickness to represent the intensity and scale of segregation, respectively. Conflicting trends are revealed in the experiments, leading to the development of an areal-based distribution of mixing intensity. For two-fluid blending, the addition of a high viscosity stream into the lower viscosity main flow causes very poor mixing performance, with unmixed spots of this component observable in the PLIF image.* © 2013 The Authors AIChE Journal published by Wiley Periodicals, Inc. on behalf of American Institute of Chemical Engineers *AIChE J*, 60: 332–342, 2014
Keywords: scale and intensity of segregation, mixing performance, PLIF, non-Newtonian fluid blending, static mixer

Introduction

Many process industry sectors, including food, home and personal care, catalyst and plastic manufacture, are tasked with the blending of highly viscous or non-Newtonian materials, often incorporating multiple immiscible phases. Applications include the blending of concentrated solid–liquid slurries, polymerizations, and the dissolution of solids or surfactants into liquids to form gels or complex surfactant/fluid phases. Due to the high apparent viscosities of some of these materials, the blending is performed under conditions which are predominantly laminar, which presents difficulties due to the lack of eddy diffusion which would assist mixing operations if the flow was turbulent.[1]

Overcoming this challenge has led to development of mixing strategies which aim to introduce chaotic flow to improve the performance; these have been employed in both batch stirred vessels[2] and inline continuous static mixers[3] which have been in use since the 1950s. Due to the complexity of the resultant flow fields formed in stirred vessels, substantial experimental and numerical studies on chaotic mixing have been undertaken to illustrate its potential to improve mixing.[2,4] Experimental work has focused on the use of optical flow diagnostic methods such as Particle Image Velocimetry (PIV) or (Planar) Laser Induced Fluorescence (PLIF)[4] on transparent systems, which have enabled the development of methods to quantify mixing performance as a function of the flow field and fluid viscosity. Modeling has involved direct numerical solution of the Navier–Stokes equations (DNS), as well as other forms of computational fluid dynamics (CFD).[5] More recent work has extended these approaches to consider the blending of non-Newtonian fluids in stirred vessels, focusing on yield stress fluids.[6] This approach has raised understanding from an empirical level, where the entire mixing quality is based upon a single measured or derived parameter, to a multi-dimensional problem which considers the spatial distribution of mixing quality as a function of the fluid flow field and rheology.

In contrast, despite the industry drive toward continuous processing due to its improved sustainability (reductions in inventory and plant footprint), there has been little effort in obtaining equivalent understanding of non-Newtonian blending within continuous inline static (motionless) mixers, though limited design information for the blending of Newtonian fluids is in the public domain.[3] The blending of non-Newtonian fluids is complicated by a nonlinear relationship between the applied shear stress and the shear rate obtained within the fluid. Newtonian design equations rely on the linear coupling between these quantities described by Newton's

Correspondence concerning this article should be addressed to M. J. H. Simmons at m.j.simmons@bham.ac.uk.

law of viscosity. Mixing quality relationships are expressed in terms of a pipe-averaged shear rate, $\dot{\gamma}$, which for the flow of a Newtonian fluid can be determined as

$$\dot{\gamma} = \frac{KV}{D} \tag{1}$$

where K is a constant (equal to 8 for a plain pipe and 28 for a KM static mixer used later in this study), V is the superficial pipe velocity, and D is the pipe diameter. For different types of static mixer, equivalent values of K are quoted which compensate for the increased wetted perimeter due to the mixer internals; increased dissipation due to changes in flow pattern (fluid deformation, stretching, and folding) and changes in fluid drag forces cause increased pressure drop over a plain pipe.[3] This shear rate is thus related to the pressure drop per unit length, a measure of the energy input to the fluid to obtain the required mixing and L/D, where L is the length of static mixer and D the diameter. Clearly, this approach is fundamentally flawed for non-Newtonian systems as Eq. 1 is no longer valid and any extrapolation must be carefully checked.[7]

The above parameters are usually related to the mixing performance expressed in terms of a coefficient of variance, CoV, (or the log variance). The CoV is defined as

$$\mathrm{CoV} = \frac{\sigma}{\overline{C}} \tag{2}$$

where σ is the standard deviation and $\overline{C}$is the average of the property (e.g., concentration) used to characterize the mixing through the device. Literature correlations[3] may be found which relate CoV to the length of static mixer required

$$\mathrm{CoV}_r = \frac{\mathrm{CoV}}{\mathrm{CoV}_0} = K_i^{\frac{L}{D}} \tag{3}$$

where CoV_0 is initial coefficient of variance in the unmixed material and CoV is the coefficient of variance required by the mixing duty. CoV_r is the ratio of these two quantities, thus expressing the reduction in CoV required by the process. K_i is 0.87 for a Kenics KM static mixer in Newtonian laminar flow.

The CoV is often used as the sole criterion for characterizing mixing efficiency or performance. However, the reality is much more complex as while CoV gives a measure of the range of a mixing property after a mixing operation, this is only one dimension of the problem. Kukukova et al.[8] proposed segregation, which may be thought of as the degree to which a material is unmixed, as being composed of three separate dimensions. The first dimension is the "intensity of segregation," which can be quantified by the CoV or alternatively by the log variance (LogVa) of concentration[8]

$$\log \mathrm{Va} = \log \sigma^2 = \log \left[\frac{1}{N-1} \sum_{i=1}^{N} [C-1]^2 \right] \tag{4}$$

where C is the normalized mixing quantity and N is the number of instantaneous measurements made on the mixing system. The second dimension is the "scale of segregation," a length scale which for a static mixer can be related to the thicknesses of the striations produced.[9] The third is the exposure or the potential to reduce segregation. Choice of which mixing criterion is most important is often dictated by the downstream process, for example, a downstream reactor may require minimization of concentration gradients to ensure adequate control of product quality, in which case control of CoV is of greatest importance. Conversely, creation of a pre-emulsion passing into a downstream emulsification process may rely on control of maximum particle size and therefore scale of segregation is most critical.

This multi-dimensional approach has not yet been applied to determine mixing quality for non-Newtonian flows in static mixers. Of the limited information available in the open literature, work has generally focused on pressure drop measurements for time independent[10–12] and viscoelastic[13] non-Newtonian fluids in static mixers with only a few recent studies examining them in more detail.[13]

In this paper, a PLIF-based method is used to characterize blending of non-Newtonian fluids in a Kenics KM mixer as function of number of mixer elements (6 and 12 elements) and fluid rheology. The transparent model fluids used are a Newtonian fluid (aqueous solution of glycerol) and two time-independent shear thinning fluids (aqueous solution of Carbopol 940 polymer) whose behavior may be described using the Herschel–Bulkley model. The blending of two fluids is explored via addition of a secondary flow at the mixer inlet which has a volumetric flow equal to ~10% of the main flow, enabling the blending of fluids with different rheologies. As in previous work,[4] the PLIF method is performed by doping the secondary fluid phase with fluorescent dye at the mixer inlet; the mixing pattern is thus obtained from images taken from a transverse section across the outlet of the mixer. From the images obtained, the scale and intensity of segregation are determined via calculation of values of LogVa and striation thicknesses respectively. A new criterion based on areal analysis of regions in the image with the same mixing intensity is proposed which combines aspects of both intensity and scale of segregation. Examination of these areal-based distributions of mixing intensity enables a deeper understanding of the complexity of the mixing to be elucidated which has the potential to provide useful information for process designers.

Materials and Methods

Static mixer experimental rig

Figure 1a shows an overall schematic of the experimental rig with Figure 1b giving a detailed schematic of the static mixer test section. A KM static mixer of diameter 12.7 mm (0.5″) with either 6 single blade 180° twisted elements or 12 elements is used, with lengths of 0.27 m ($L/D = 21$) and 0.53 m ($L/D = 42$), respectively. Operational superficial velocities for static mixers range from 0.1 to 1 m s^{-1}. In this work, a constant total superficial velocity of 0.3 m s^{-1}, corresponding to a total volumetric flow rate of 184 L h^{-1}, was used in all PLIF experiments. The primary flow is delivered by a Liquiflo gear pump at $Q = 160$ L h^{-1}, controlled using a motor drive (Excal Meliamex) and monitored using an electromagnetic flow meter (Krohne). A secondary flow is introduced using a Cole-Palmer Micropump (GB-P35) at $Q = 24$ L h^{-1} and the injection position is located one pipe diameter distance from the first static mixer element; details of the injector design are shown in Figure 1c. This flow is doped with fluorescent dye (Rhodamine 6G).

To enable flow measurements to be made using PLIF, which requires optically transparent materials, a Tee piece is placed at the end of the mixer section which has a glass window inserted on the corner of the Tee, normal to the axis of the main pipe. A glass pipe section upstream of the Tee at the mixer section outlet provides optical access for the laser sheet to illuminate the transverse section which is located one pipe diameter downstream from the last element of static mixer.

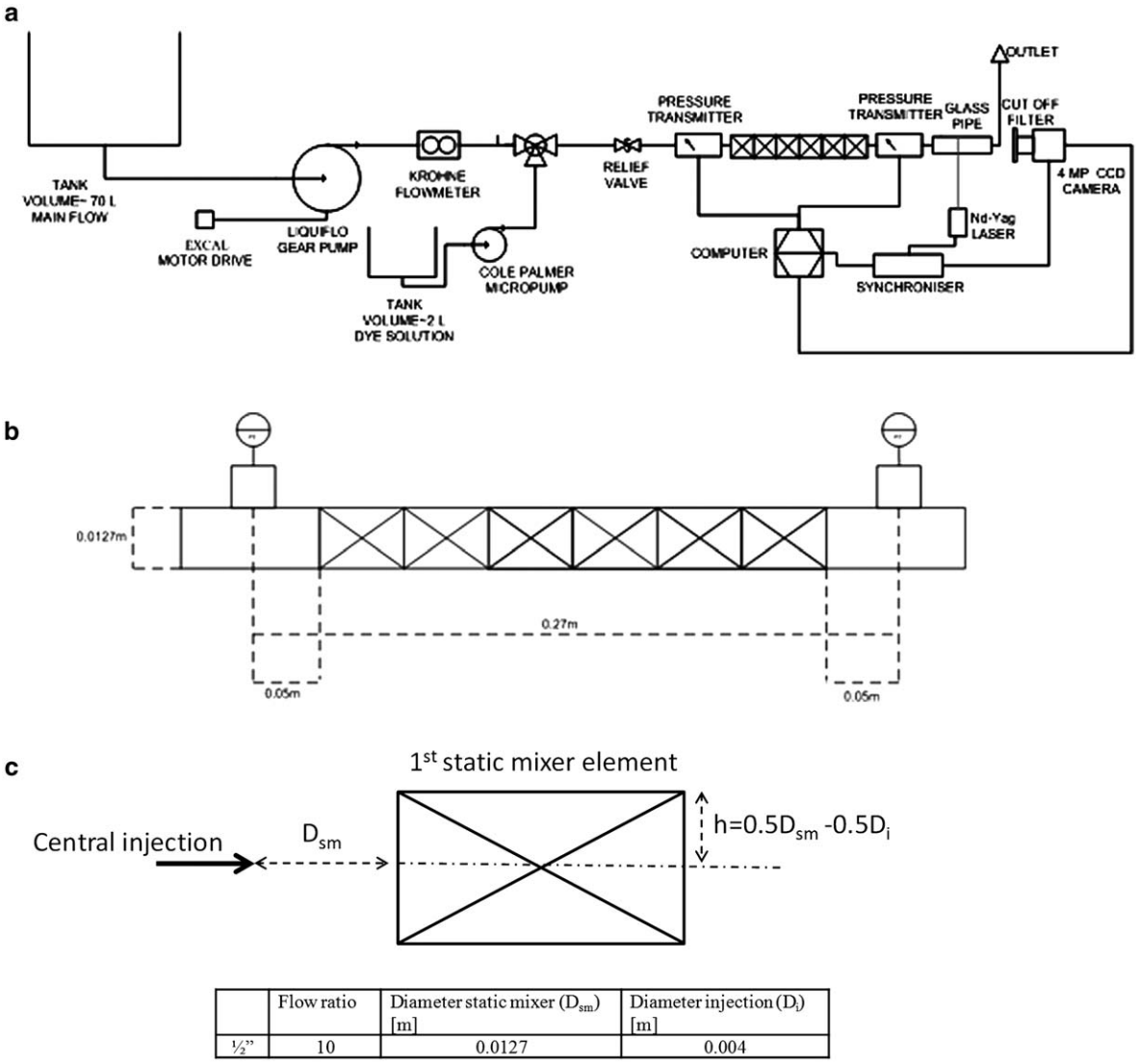

	Flow ratio	Diameter static mixer (D_{sm}) [m]	Diameter injection (D_i) [m]
½"	10	0.0127	0.004

Figure 1. Schematics of the static mixer test rig.

(a) Overall schematic, (b) dimensions of static mixer test section showing location of pressure transducers; and (c) injection positions.

Two pressure transmitters were located both upstream (PR-35X / 10 bar, Keller UK) and downstream (PR-35X / 1 bar, Keller UK) of the static mixer section, enabling measurement of the pressure drop at a sampling rate of 5 Hz. The transducers were placed as close as possible to the mixer section being mounted four pipe diameters before and after the section, respectively (Figure 1b). The pressure transmitters also incorporated PT100 thermocouples enabling the temperature of the fluids to be monitored throughout the experiments. The temperature of the fluids was maintained at 22°C to ensure the rheology of the fluids remained constant. Pressure drop data was obtained for both fluids without injection (fluids 1 and 2 considered as primary fluids) over a range of superficial velocities from $0.1 < V < 0.6$ m s^{-1} ($60 < Q < 300$ L h^{-1})

Fluids and flow conditions

The working fluids are aqueous solutions of glycerol or Carbopol 940 (Lubrizol Corp, OH), a cross-linked polyacrylate polymer. The rheology of all fluids was obtained using a cone and plate rheometer (TA AR1000, TA Instruments) equipped with a 40 mm diameter 2° steel cone. The aqueous Carbopol 940 solutions were found to be well represented by the Herschel–Bulkley model over a range of shear rate, $\dot{\gamma}$ from 0.1 to 1000 s^{-1}, as found previously,[14] shown in Figure 2

$$\begin{aligned} \dot{\gamma} &= 0 \quad \text{for } \tau < \tau_0 \\ \tau &= \tau_0 + k\dot{\gamma}^n \quad \text{for } \tau > \tau_0 \end{aligned} \tag{5}$$

where τ is the shear stress, τ_0 is the yield stress, k is the consistency index, and n is the power law exponent. The physical properties of the fluids are given in Table 1.

Three different flow conditions were selected as shown in Table 2. Experiment #1 involved use of the Newtonian glycerol solution ("fluid 1") for both primary and secondary flows, thus providing a baseline for comparison with published data. Experiments #2 and #3 used the non-Newtonian Carbopol solutions. Experiment #2 used the non-Newtonian "fluid 2" for both flows. Experiment #3 explored mixing of fluids with different rheology by using "fluid 2" for the primary flow and the more viscous "fluid 3" for the secondary flow. Each experiment was performed using both 6 and 12 KM mixing elements.

Table 1. Physical Properties of the Aqueous Solutions Used in the Experiments

	Density, ρ (kg m^{-3})	Yield Stress, τ_0 (Pa)	Power Law Exp., n (-)	Consistency Index, k, (Pa s^{n-1})	Viscosity at Wall Shear Rate, μ_w, (Pa s)	pH (-)
Fluid 1: 80% wt Glycerol	1200	–	–	–	0.05	–
Fluid 2: 0.1% wt Carbopol 940	1000	3.2	0.7	0.26	0.05	4.5
Fluid 3: 0.2% wt Carbopol 940	1000	25.2	0.42	6.74	0.20	5

The Reynolds number for the flows, based on a plain tube, is calculated as

$$\mathrm{Re} = \frac{DV\rho}{\mu} \tag{6}$$

leading to a value of 88 for the Newtonian Experiment #1. Although transitional values of Reynolds number are somewhat dependent upon the geometry, this calculated value is well below those available in the literature, which quote values in the range of $\mathrm{Re} > 500$.[15] Calculation of Reynolds number for the non-Newtonian fluids is more complex as the viscosity is a function of shear rate. To provide an initial estimate for Experiments #2 and #3, the apparent viscosity of fluid was calculated at an average shear rate obtained using Eq. 1 with $K = 28$ ($\dot{\gamma} = 650\ \mathrm{s}^{-1}$), corrected for a shear thinning fluid[16] by multiplying by $(3n+1/4n)$. The values of Re obtained were 88 and 91, respectively, confirming the flow was laminar.

PLIF measurements

The two-dimensional PLIF measurements were performed using a TSI PIV system (TSI). The system comprises of a 532 nm Nd-Yag laser (New Wave Solo III) pulsing at 7 Hz, synchronized to a single TSI Powerview 4MP (2048 × 2048 pixels) 12 bit CCD camera using a synchronizer (TSI 610035) attached to a personal computer. The PIV system was controlled using TSI Insight 4G software.

The camera is equipped with a 545 nm cut-off filter to eliminate reflected laser light so that only the fluorescent light emitted by the dye ($\lambda = 560$ nm) excited in the measurement plane is captured on the image. The spatial resolution of the measurements was 10 μm pixel^{-1}. The system was calibrated by filling the entire pipe volume with Rhodamine 6G dye solutions at three different concentrations (0.1 mg L^{-1}, 0.5 mg L^{-1}, and 1 mg L^{-1}) at fixed laser power. A pixel by pixel calibration was then performed using MATLAB for each concentration which confirmed a linear relationship between the dye concentration and the measured grayscale value over this range.[17] For the subsequent PLIF experiments, the concentration of the dye in the secondary flow was thus selected as 0.5 mg L^{-1} to ensure all measurable concentrations in the mixing section were within the linear range.

Both advection and molecular diffusion are relevant possible mixing mechanisms in these experiments, although due to the viscous nature of the fluids (Table 1) it would be expected that advection would be the dominant mechanism as the value for Schmidt number, $\mathrm{Sc} = \upsilon/D_M >> 1$ for all the experiments.[1] The spatial concentration distributions obtained in the PLIF images nevertheless arise from mixing by both mechanisms and are resolved to 10 μm. It is not possible to decouple the mixing effects due to each mechanism from the PLIF images.

To assess the temporal variation of the images, 10 images were acquired in three batches spaced several minutes apart for each experiment. No temporal variation was observed in any of the experiments, confirming the mixer was operating at steady state.

Table 2. Summary of Experimental Conditions

Experiment #	#1	#2	#3
Primary flow	Fluid 1	Fluid 2	Fluid 2
Secondary flow	Fluid 1	Fluid 2	Fluid 3

Characterization of Mixing Performance Using PLIF Data

The overall strategy for evaluation of mixing performance from the PLIF images is shown in Figure 3. In addition to calculation of the usual measures of mixing performance (LogVa and striation thickness), a new method to obtain an areal distribution of mixing intensity is proposed.

CoV, LogVa, *and striation thicknesses*

CoV and LogVa were calculated by analysis of the PLIF images using an algorithm developed in MATLAB. The images were imported into MATLAB and converted into a 2048 × 2048 matrix with each element in the matrix corresponding to a pixel in the image. With the 12 bit camera used, each element contains an integer number between 0 (black) and 4095 (white). The region within the matrix corresponding to the pipe cross section was isolated and the number of elements in this region N, was counted. CoV and LogVa were then determined using Eqs. 2 and 4, respectively, defining the mixing property, C, as the dimensionless concentration

$$C = \frac{C_i - C_0}{C_\infty - C_0} \tag{7}$$

where C_0 is the background value obtained from the calibration ($C_0 \rightarrow 0$), C_i is the measured concentration in element

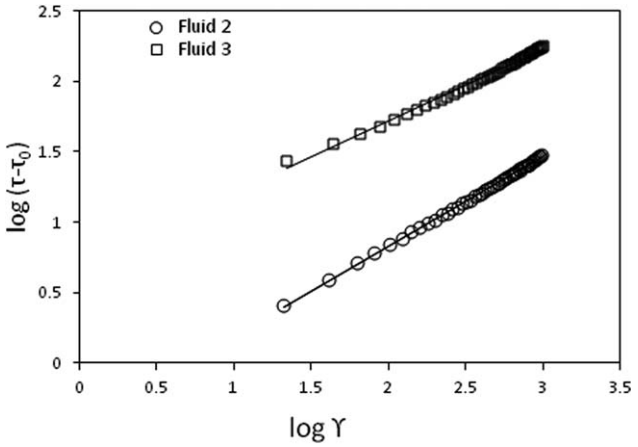

Figure 2. Rheology of the non-Newtonian fluids used (fluids 2 and 3, Table 1) fitted to the Herschel-Bulkley model.

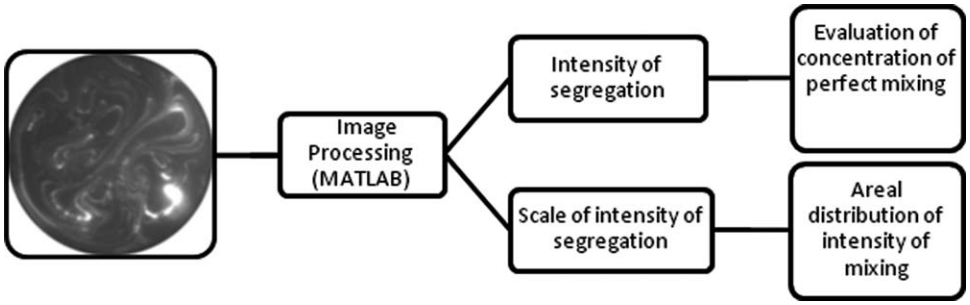

Figure 3. Block flow diagram showing analysis methods applied to the PLIF images.

i and C_∞ is the fully mixed concentration assuming perfect blending of the dye, which corresponds to the average concentration in the image.

The striation thickness distribution was determined using a MATLAB algorithm which performed a row by row (or column by column) analysis of the imported image matrix. The number of contiguous pixels with the same grayscale value (within a predefined tolerance) and thus within the same striation were counted and converted to a length via calibration (10 μm pixel^{-1}). This automated method was used due to the difficulty of manual analysis of the data. A limitation of the method is that it does not identify if individual striations in adjacent rows or columns are within the same striation. This weights the distribution in favor of the larger striations, as they occupy a larger cross-sectional area. Although these data are not therefore absolute, the method does allow relative comparisons between the different experiments.

Areal distribution of mixing intensity

An alternative method of examining the mixing performance is proposed based on analysis of areas (striations) within the PLIF image which possess the same level of mixing, leading to an areal distribution of mixing intensity over the image. This method is described with reference to Figure 4; Figure 4a displays a typical distribution of grayscale values (which are proportional to dye concentration) which would be obtained from an image such as that shown in Figure 4b. Plug flow is assumed in the image analysis, so that each pixel is of the same importance. Thus, the mean value of grayscale in the image (corresponding to the fully mixed concentration,C_∞), $\overline{G}$, can be easily evaluated from the distribution. The mass balance of dye from the inlet to the PLIF measurement point can then be checked assuming that the plug flow does not drastically affect the grayscale values in the selected cross section

$$\overline{G} = \frac{F_{\text{dye}} G_{\text{dye}} + F_0 G_0}{F_{\text{dye}} + F_0} \tag{8}$$

where F_{dye} and F_0 are the volumetric flow rates of the primary and secondary flow and G_{dye} and G_0 ($G_0 \to 0$) are the grayscale values corresponding to the concentrations of dye present. The theoretical values for $\overline{G}$ calculated using Eq. 8 were within 5% of the experimentally determined values for all experiments, thus the mass balance was closed to within an error of ±5%.

Using the experimentally determined value of $\overline{G}$, it is possible to calculate grayscale values corresponding to a given level of mixedness. Taking X% mixing as an example, this corresponds to grayscale values of either $G_{X-} = [1-(1-X)]\ \overline{G}$ or $G_{X+} = [1+(1-X)]\ \overline{G}$. So for 95% mixing, $G_{X-} = 0.95\overline{G}$ and $G_{X+} = 1.05\overline{G}$. Note that from Eq. 4, both give the same log variance, as expected. Using MATLAB and the freeware image analysis tool Image J, the pixels in the image are identified which correspond to $G_{X-} < G$

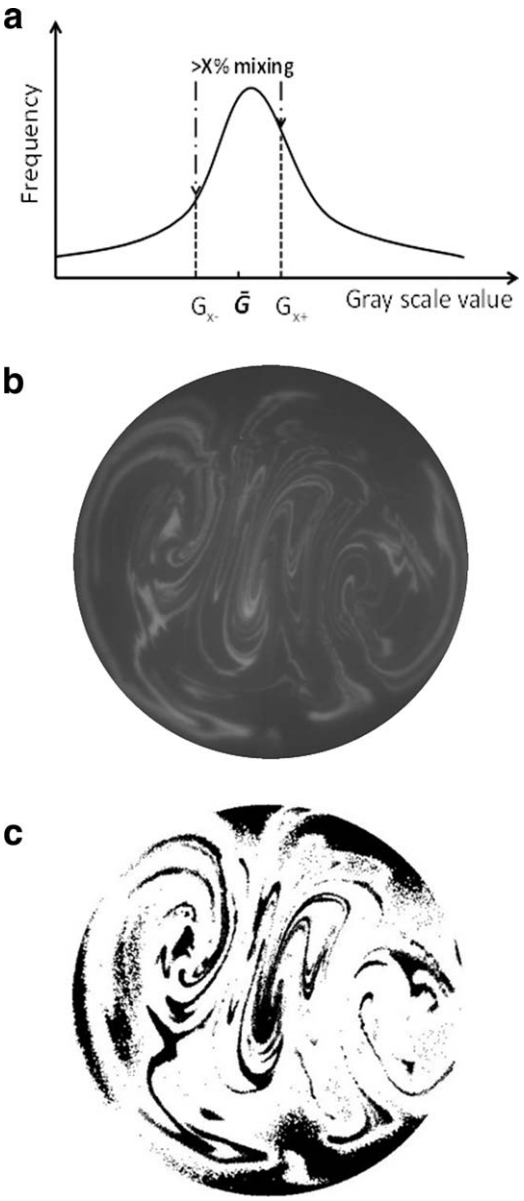

Figure 4. Development of areal analysis method.

(a) Identification of regions in the grayscale distribution with a given mixing intensity; (b) raw image; (c) example of image processing for the Experiment #1 12 elements with regions of mixing intensity > 60% in white.

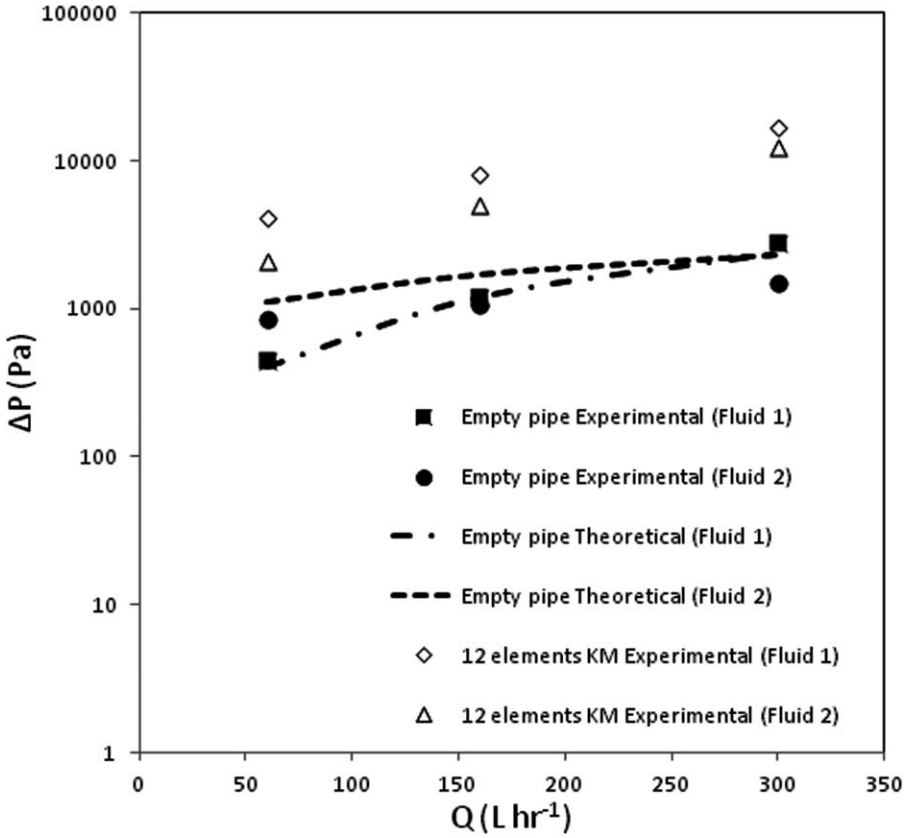

Figure 5. Pressure drop measurements made for both continuous phase fluids in the empty pipe and comparison with theoretical predictions.

$< G_{X+}$, thus corresponding to a mixing intensity of $> X\%$: this arbitrary region is shown in Figure 4a. These pixels are then set to white ($G = 4095$) in the image, with the remaining out of range pixels being set to black ($G = 0$). An example of this procedure is shown in Figure 4c, where the fraction of the total cross-sectional area corresponding to this mixing intensity is then easily determined from the fraction of white pixels. By repeating this procedure over a range of values of X, both discrete and cumulative areal distributions of mixing intensity are thus obtained.

Results and Discussion

Pressure *drop*

The pressure drops, ΔP, measured over an empty pipe for both continuous phase fluids, fluid 1 and fluid 2, are plotted in Figure 5 and compared with theoretical values obtained from Eq. 9 for fluid 1 and Eq. 10[16] for non-Newtonian fluid 2

$$Q = \frac{\pi D^4 \Delta P}{128 \mu L} \tag{9}$$

$$Q = \frac{8\pi L^3}{\Delta P^3}\frac{1}{k^{1/n}}\left[\frac{n}{3n+1}\left(\left[\frac{\Delta P}{L}\frac{R}{2}\right]-\tau_y\right)^{\frac{3n+1}{n}} + \frac{2\tau_y n}{2n+1}\left(\left[\frac{\Delta P}{L}\frac{R}{2}\right]-\tau_y\right)^{\frac{2n+1}{n}} + \frac{\tau_y^2 n}{n+1}\left(\left[\frac{\Delta P}{L}\frac{R}{2}\right]-\tau_y\right)^{\frac{n+1}{n}}\right] \tag{10}$$

where Q is the volumetric flow rate and μ is the dynamic viscosity of the Newtonian fluid. Excellent agreement is observed for the Newtonian fluid and good agreement is observed with the non-Newtonian fluid, apart from at very low flow rates. Values of pressure drop for the same fluids in the empty pipe and after 12 KM mixer elements are given in Table 3. K_L values for the KM mixer are thus derived using Eq. 11

$$\Delta P_{sm} = \Delta P_{empty} K_L \tag{11}$$

The K_L value of 6.77 for the Newtonian fluid agrees well with the literature value[7] of 6.9. Although this approach is not applicable for the non-Newtonian fluid due to the Herschel–Bulkley constitutive law, the value of $K_L = 4.77$ is significantly different from the Newtonian value. Notably, the pressure drops obtained from Experiments #2 and #3 are quite similar, despite the addition of the minor flow of fluid 3 in Experiment #3.

Images obtained from PLIF technique

Raw PLIF images obtained from each experiment are shown in Figure 6. The images show the distribution of dye tracer in the cross section of the pipe after both 6 and 12 elements of KM static mixer for each experiment. In the case of Newtonian blending (Experiment #1), there is a notable reduction in the observed striation thickness when the number of elements is increased (Figures 6a, b), with the overall mixing pattern showing evidence of stretching and folding which is typical for KM static mixers.[18] A bright spot of dye is observable in the bottom right hand corner of the image in Figure 6a suggesting some bypassing of the dye stream; however, this is no longer noticeable in Figure 6b, after an additional 6 KM elements.

Table 3. Pressure Drops over Empty Pipe (0.53 m) and 12 KM Mixer Elements (0.53 m) for the Continuous Phase Fluids (Fluid 1 and Fluid 2)

	Pressure Drop, ΔP (Empty Pipe) (Pa)	Pressure Drop, ΔP (12 KM Elements) (Pa)	Calculated Value of K_L From Eq. 11
#1 (Newtonian)	1200	8122	6.77
#2 (non-Newtonian)	1060	5040	4.77
#3 (non-Newtonian)	1120	5200	4.64

For the non-Newtonian blending experiment, a similar reduction in striation thickness is observed when the number of elements is increased (Figures 6c, d). However, the pattern of striations is markedly different. As the flow conditions between Experiments #1 and #2 are identical, the differences must be due to the fluid rheology which leads to a different distribution of shear stresses, and thus shear rates and velocities, within the mixer geometry which manifests itself as changes in the striation patterns.

A dramatic change in mixing behavior is observed for Experiment #3. No mixing at all is observed after six elements (Figure 6e), and the dye remains as a central bright spot as injected into the mixer. This suggests that the dye stream has bypassed the elements. However, after 12 elements (Figure 6f), some splitting has occurred as the majority of the stream has been "shattered" into a series of smaller bright spots. Some of the stream has, however, been blended by the mixer, leading to a conventional mixing pattern with thin striations observable in the background.

Analysis of *mixing performance* from PLIF *images*

Values of CoV determined for all experiments using Eq. 2 are given in Table 4. Notable differences are observed between each experiment, unsurprisingly Experiment # 3 gives by far the worst performance. Comparison of experimental values of CoV_r with Eq. 3 with $K_i = 0.87$, shows good agreement for the Newtonian case (#1). CoV_0 was calculated based on the unmixed volume fraction at the inlet $C_v = 0.13$ using[3]

Table 4. CoV_r From Experimental Data and Eq. 3

	Measured CoV	Measured $CoV_r = \frac{CoV}{CoV_0}$	Theoretical $CoV_r = K_i^{\frac{L}{D}}$
#1 6 elements	0.156	0.006	0.052
#1 12 elements	0.089	0.003	0.003
#2 6 elements	0.264	0.101	0.052
#2 12 elements	0.089	0.003	0.003
#3 6 elements	0.484	0.186	0.052
#3 12 elements	0.193	0.074	0.003

$$CoV_0 = \left(\frac{1-C_v}{C_v}\right)^{0.5} = 2.6 \tag{12}$$

Figure 7 gives a comparison of the measured CoV with the CoV data obtained by Alloca and Streiff[7] for a KM mixer blending Newtonian fluids where flow rate is 10% of the main flow, close to that in this work. Their range of L/D covers Experiment #1 with six elements where L/D is ~21. Their value of CoV is ~0.2 which is very close to the value of CoV = 0.17. Extrapolating their data to an L/D of 42 produces a CoV which is a conservative estimate of the result obtained from this study.

It is of interest to consider the mixing performance of the experiments in terms of the mechanical energy input to the process, as from an industrial perspective this defines the size of the pump and thus capital and running costs. Experimental and theoretical values of CoV from Table 4 are plotted in Figure 8 versus the energy inputted into the flow per unit mass of pumped fluid, expressed as the measured $\Delta P/\rho$ (J kg^{-1}),where ρ is the fluid density. Clear differences in the degree of mixing obtained are observed for each of the experiments. As this parameter does not include viscosity ratio it does not collapse the data: Experiments #2 and #3 have ostensibly the same pressure drop (Table 3), sharing

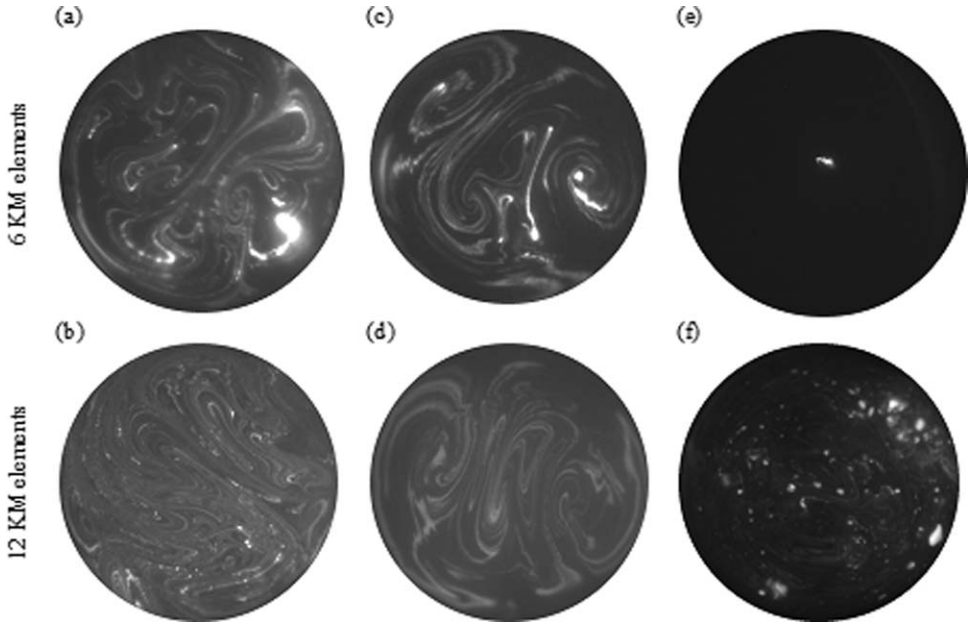

Figure 6. Raw PLIF Images.

(a) and (b) show #1 for 6 and 12 elements; (c) and (d) show #2 for 6 and 12 elements, and (e) and (f) show #3 for 6 and 12 elements, respectively.

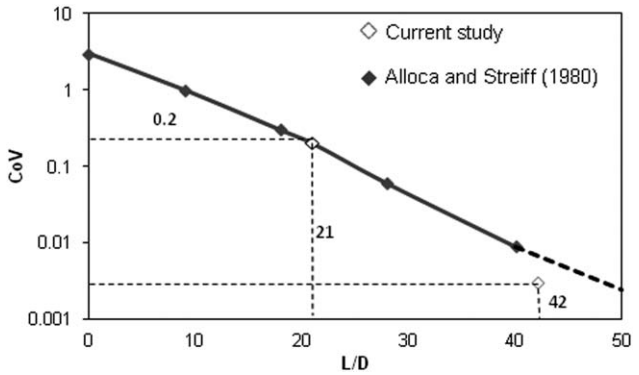

Figure 7. Coefficient of variance (CoV) data from Alloca and Streiff[7] compared with the present study.

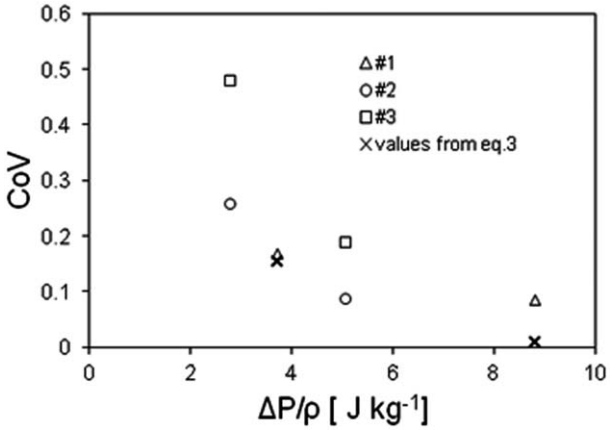

Figure 8. CoV versus $\Delta P/\rho$ for all the experiments developed for this work compared with Eq. 3.

the same continuous phase, yet a very different mixing performance is observed. Overall, Experiment #1 and Experiment #3 give the best and worst performance, as before. Theoretical values of CoV using Eq. 3 show some agreement with data from Experiment #1. It is clear that existing published data cannot account for the effects of non-Newtonian rheology or viscosity ratio.

Kukukova et al.[8] described the complexities of mixing processes and highlighted the need to consider a multi-dimensional approach to the problem, including the intensity and scale of segregration. The intensity (LogVa) and scale of segregation (maximum striation thickness) are plotted in Figures 9a, b, respectively, as a function of the number of KM mixer elements. Figure 9a shows that, unsurprisingly, values of LogVa decrease significantly when the number of mixing elements increases for all experiments. The final values produced are a function of the fluid rheology in all cases, apart from the agreement between Experiments #1 and #2 when 12 elements are used. In contrast, the average striation thicknesses (Figure 9b) show a different trend. It should be noted that the thicknesses of the measured striations are all much larger than the resolution of the PLIF camera. Remarkably, Experiment #3 gives the "best" performance with the lowest average striation thickness for 12 elements. This can be explained by the relatively few striations in Experiment #3 skewing the striation distributions, due to lack of mixing and no distinction between striations where the fluids are mixed or where there is no mixing at all. This reinforces the danger of only considering either LogVa or striation thicknesses in isolation when determining overall mixing quality[6] and has led to the development of the approach proposed below which considers both the scale and intensity of segregation in conjunction.

Areal *distribution* of *mixing intensity*

Images obtained from the areal-based analysis are given in Figure 10 for each experiment when performed using 12 KM mixing elements. The images show the areal regions corresponding to discrete distributions of intensity, X, as shown, between $60\% < X < 100\%$. Examining the images in Figure 10 further, white areas can be identified which are individual striations consistent with those observable in Figure 6. This is as would be expected from the mixing mechanism of stretching, cutting, and folding which will produce striations with a similar CoV or log variance. However, the analysis is not capable of determining the boundaries of

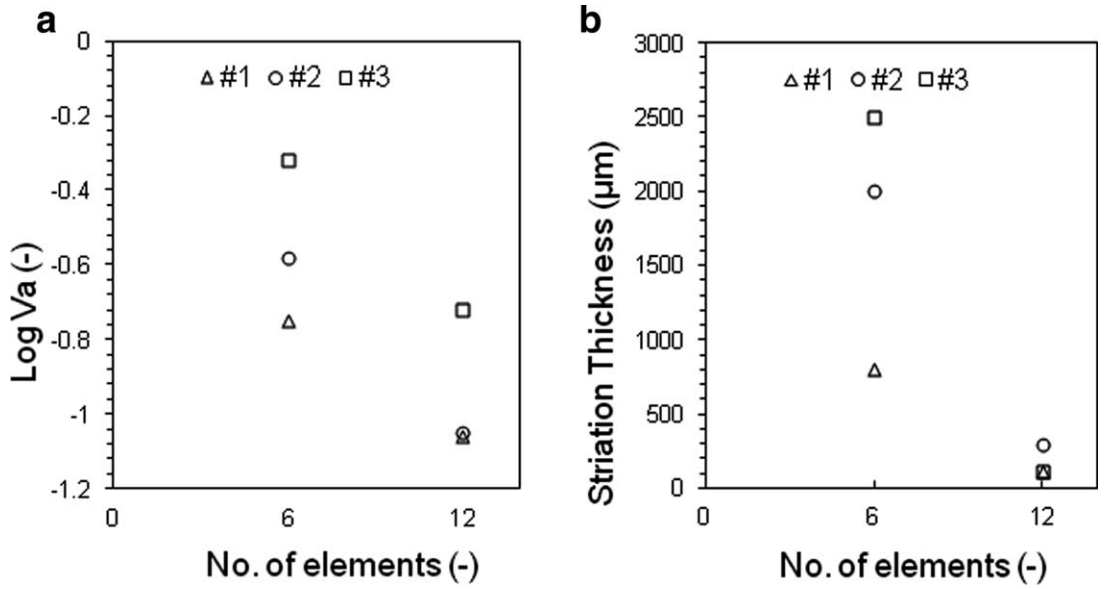

Figure 9. Comparison of (a) intensity (log variance) and (b) scale of segregation (maximum striation thickness) obtained from the PLIF analysis.

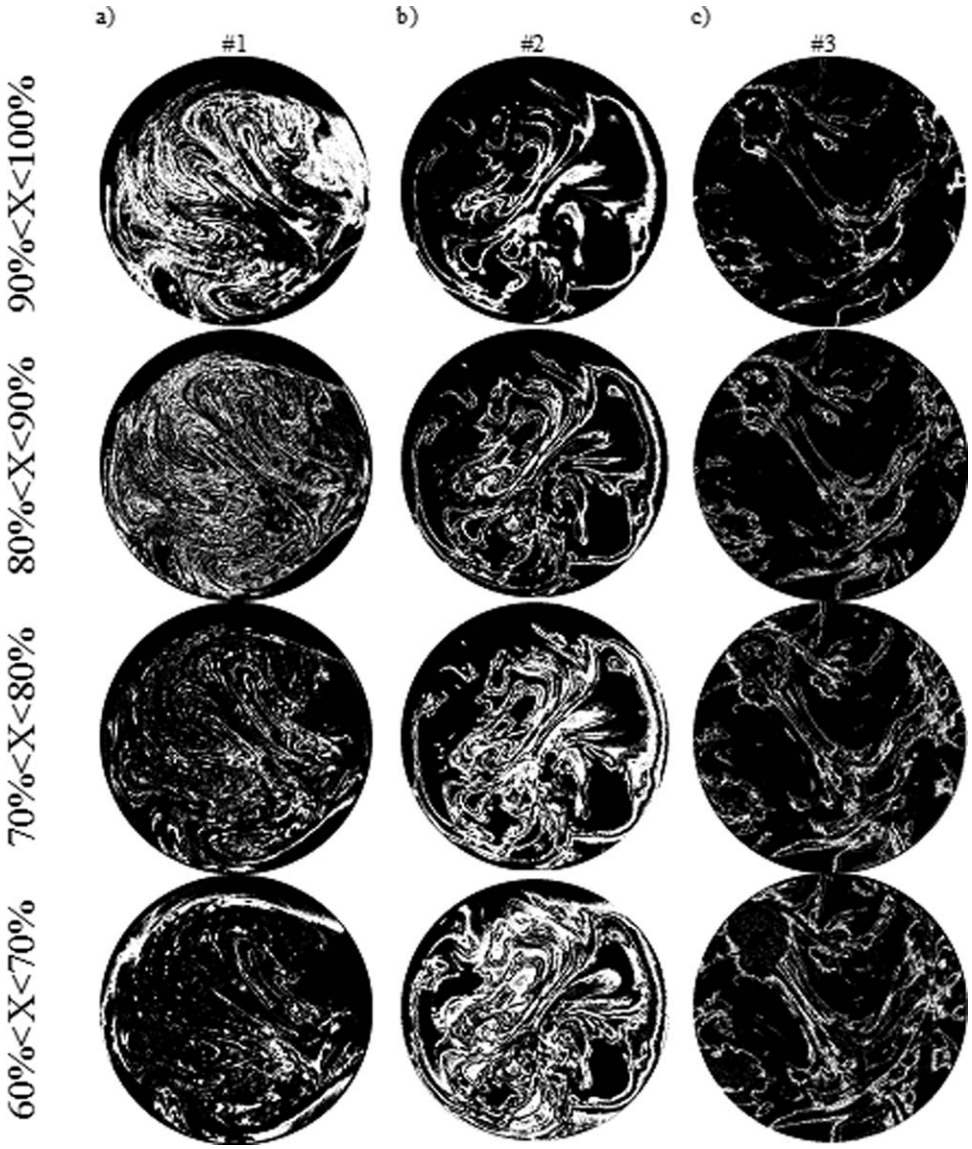

Figure 10. Application of the areal mixing analysis to the PLIF images obtained for 12 KM mixing elements.

Discrete distributions are shown for (a) Experiment #1, (b) Experiment #2, and (c) Experiment #3, respectively. Areas in white are within the range of interest.

individual contiguous striations (which would be a useful future development) as it only considers the intensity values on a pixel by pixel basis.

It is notable in all the images in Figures 6 and 10 that there is an alignment of the striations with the blade of the last element, which runs from the top left to the bottom right in all of the images. However, the striation distributions are not symmetrical from one side of the mixer to the other. This is most apparent for the non-Newtonian experiments shown in Figures 10b, c and may be reflective of nonlinearities introduced by the non-Newtonian rheology. Large black areas corresponding to unmixed regions ($X < 60\%$) are observable, these may be suggestive of regions where the fluid is traveling as a solid plug, with relatively low shear rates due to the yield stress and shear thinning nature of the fluid; however this cannot be proven without a full three-dimensional flow simulation or experimental measurement. These regions are again much larger than for the Newtonian case. The distributions show that regions with mixing >90% are confined to a few striations which appear to be relatively thick compared with the large numbers of thin striations corresponding to lower mixing levels (e.g., $60\% < X < 70\%$). Regions of mixing intensity close to 100% would be identifiable as those where the mixing has led to homogeneity to within 10 μm (the resolution of the experiments).

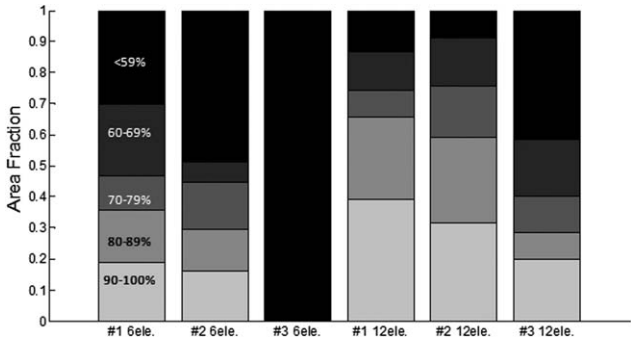

Figure 11. Bar graph showing discrete areal intensity distributions for each experiment.

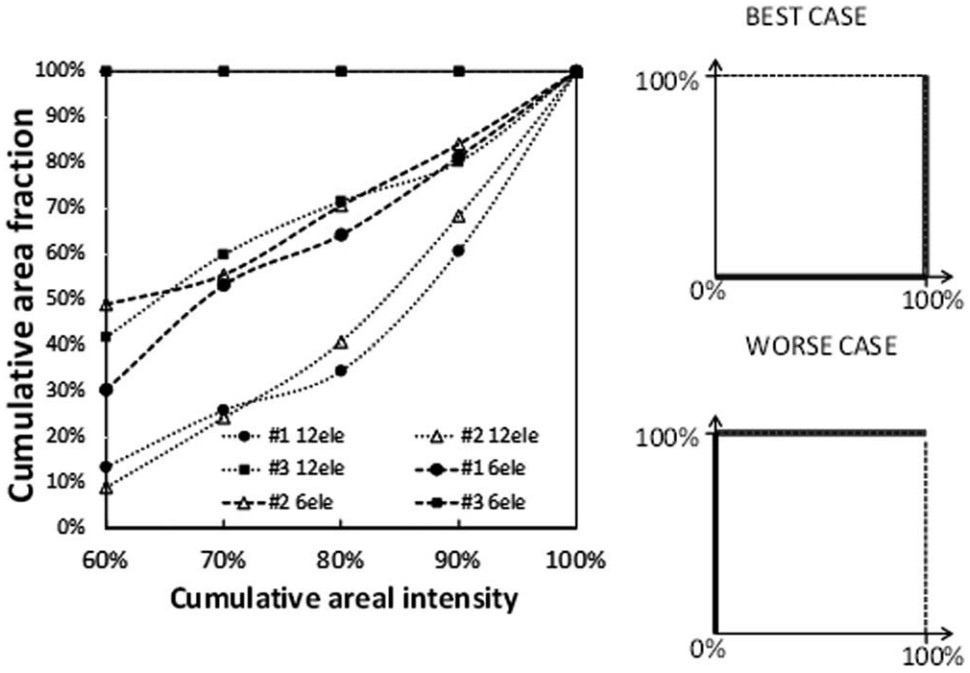

Figure 12. Cumulative areal intensity distributions as a means of determining relative mixing performance between experiments.

The discrete distributions of area fraction as a function of mixing intensity are plotted as a bar graph in Figure 11. This presentation enables quantification of the mixing performance between each experiment and shows the improvement in all cases when 12 KM elements are used instead of six elements. The areal fraction for $X > 90\%$ approximately doubles from 19% to 39% for Experiment #1; corresponding values for Experiment # 2 are 15% and 32% for 6 and 12 elements, respectively. As no mixing occurred for Experiment #3 when 6 KM elements are used (Figure 6e), this is reflected in an overall mixing intensity $<59\%$ across the whole cross section. An alternative visualization of the data

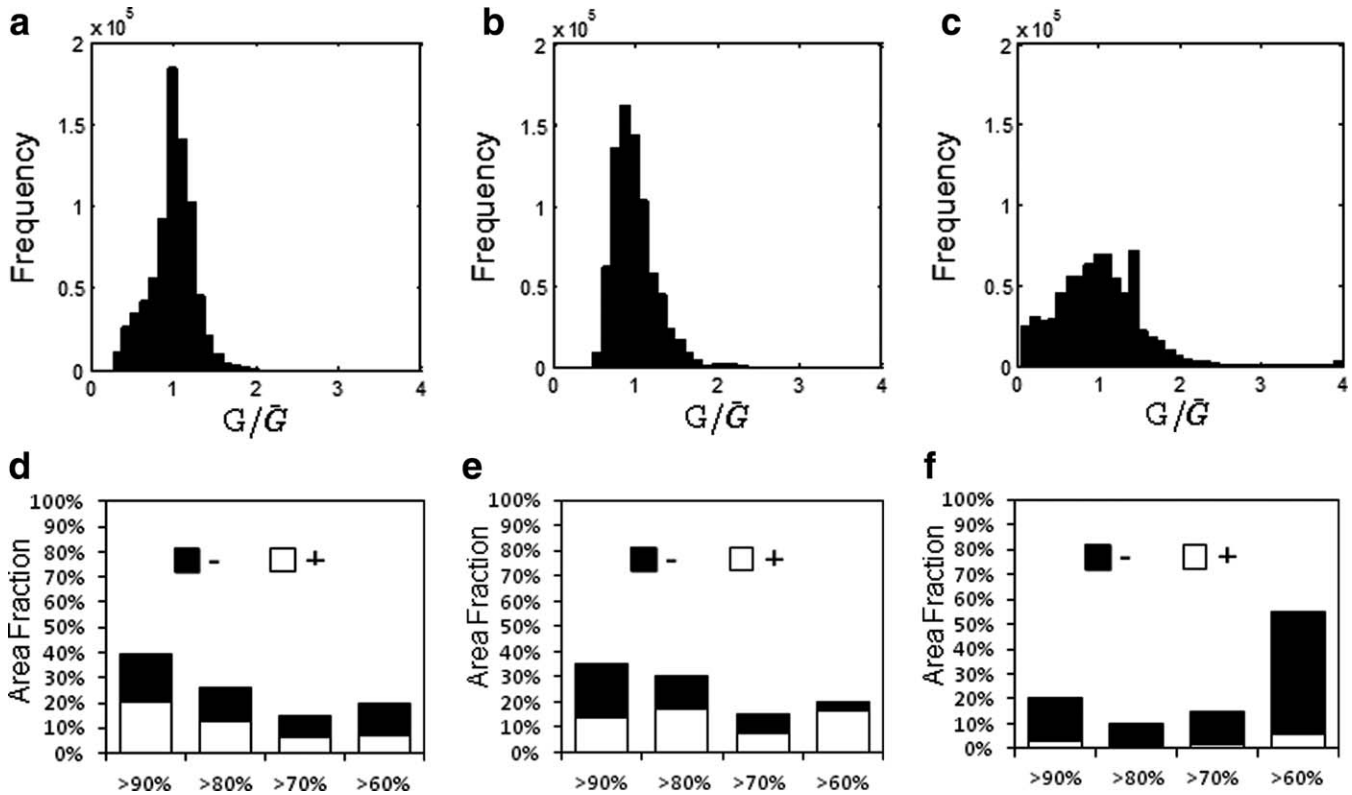

Figure 13. Grayscale distributions for (a) Experiment #1, (b) Experiment #2, and (c) Experiment #3, all carried out with 12 KM elements.

Sub figures (d), (e), and (f) show the breakdown of area fraction due to G_{X-} and G_{X+} for Experiments #1, #2, and #3, respectively.

is given using the cumulative distributions plotted in Figure 12, where the overall performance can be assessed compared with the idealized cases of 100% mixing (best case) and 0% mixing (worst case) given on the right hand side of the figure. This presentation enables the mixing performance between the experiments to be ranked as: #1 12 elements > #2 12 elements > #1 6 elements > #2 6 elements > #3 12 elements. In performing this comparison, a higher weighting is given to the area fractions with a higher mixing intensity for the worst performing cases, as there is some overlap in the cumulative distributions.

Further insight into the mixing can be obtained by examination of the distribution of grayscale values, G, in the PLIF images, as shown in Figure 13 for the experiments performed with 12 KM elements. Grayscale distributions for Experiments #1, #2, and #3, are shown in Figures 13a–c, respectively. Values of $\overline{G}$are also marked on the figures. A greater skew in the distributions is observable for the non-Newtonian experiments, which has led to further analysis to determine the cumulative fractional contribution of both the G_{X-} and G_{X+} components for a given degree of mixing in Figures 13d–f.

The G_{X-} and G_{X+} fractions are approximately even for Experiment #1, but are biased toward the G_{X+} component for Experiment #2. Reasons for this are unclear, but may be related to the remarkably few pixels possessing low grayscale values in Figure 13b, leading to a negative skew on the distribution. For Experiment #3 (Figure 13d) the G_{X-} fraction dominates: this can be attributed to the generally poor mixing performance for this experiment, with the higher concentrations of dye being isolated in the bright spots observed in Figure 6f.

Conclusions

Analysis of PLIF images has been performed to determine the mixing performance of KM static mixers using Newtonian and non-Newtonian aqueous solutions as a function of number of elements and viscosity ratio of the two fluids. Analysis of the data using log variance for intensity of segregation and striation thickness for scale of segregation has demonstrated the importance of considering both aspects in tandem for correct interpretation of the mixing performance; considering only a single measure is a known problem in the literature.[8,9,19] A method is presented which considers the distribution of the cross-sectional area with a given intensity of mixing, this areal analysis combines both intensity, in terms of log variance, and scale, in terms of the fraction of the cross section with a given intensity. The method shows promise for the evaluation of mixing performance and can be considered as an addition to conventional approaches. The analysis does also to some extent identify striations of similar intensity, but identification of individual contiguous striations would be a useful future development. The identification of areas in the pipe cross section with a given range of log variance enables identification of regions where the mixing is performed down to the micro-scale, but also unmixed or poorly mixed regions in the flow. The analysis of PLIF images allowed the detection of viscous stream filaments evident as spots when a fluid of higher viscosity was injected into a lower viscosity continuous phase, which is not predictable using conventional design approaches. This new method shows promise in unraveling the complexity of information-rich PLIF images, beyond a sole number-based mixing criterion.

Acknowledgments

FA is funded by an EPSRC DTA studentship and Johnson Matthey. The PIV equipment was purchased using funds from EPSRC grants GR/R12800/01 and GR/R15399/01.

Literature Cited

1. Todd DB. Mixing of highly viscous fluids, polymers and pastes. In: Paul EL, Atiemo-Obeng VA, Kresta SM, editors. Handbook of Industrial Mixing: Science and Practice. Hoboken, NJ: Wiley, 2004: 987–1025.
2. Alvarez MM, Zalc JM, Shinbrot T, Arratia PE, Muzzio FJ. Mechanisms of mixing and creation of structure in laminar stirred tanks. *AIChE J*. 2002;48:2135–2148.
3. Etchells AW, Meyer CF. Mixing in pipelines. In: Paul EL, Atiemo-Obeng VA, Kresta SM, editors. Handbook of Industrial Mixing: Science and Practice. Hoboken, NJ: Wiley, 2004:391–478.
4. Arratia PE, Muzzio FJ. Planar laser-induced fluorescence method for analysis of mixing in laminar flows. *Ind Eng Chem Res*. 2004;43: 6557–6568.
5. Zalc JM., Szalai ES, Alvarez MM, Muzzio FJ. Using CFD to understand chaotic mixing in laminar stirred tanks. *AIChE J*. 2002;48: 2124–2134.
6. Patel D, Ein-Mozaffari F, Mehrvar M. Dynamic performance of continuous-flow mixing of pseudoplastic fluids exhibiting yield stress in stirred reactors. *Ind Eng Chem Res*. 2011;50:9377–9389.
7. Alloca P, Streiff FA. Difficult Mixing Session. Presented at the AIChE Annual Meeting, Chicago, 1980.
8. Kukukova A, Aubin J, Kresta, SM. A new definition of mixing and segregation: three dimensions of a key process variable. *Chem Eng Res Des*. 2009;87:633–647.
9. Kukukova A, Aubin J, Kresta SM. Measuring the scale of segregation in mixing data. *Can J Chem Eng*. 2011;89:1122–1138.
10. Shah NF, Kale DD. Pressure drop for laminar flow of non-Newtonian fluids in static mixers. *Chem Eng Sci*. 1991;46:2159–2161.
11. Fasol C, Choplin, L. Pressure drop of Newtonian and non-Newtonian fluids across a Sulzer SMX static mixer. *Chem Eng Res Des*. 1997;75:792–796.
12. Liu S, Hrymak AN, Wood PE. Laminar mixing of shear thinning fluids in a SMX static mixer. *Chem Eng Sci*. 2006;61:1753–1759.
13. Chandra K, Kale, DD. Pressure drop for laminar flow of viscoelastic fluids in static mixers. *Chem Eng Sci*. 1992;47:2097–2100.
14. Adams LW, Barigou M. CFD analysis of caverns and pseudo-caverns developed during mixing of non-Newtonian fluids. *Chem Eng Res Des*. 2007;85:598–604.
15. Hirech K, Arhaliass A, Legrand J. Experimental investigation of flow regimes in an SMX Sulzer Static Mixer. *Ind Eng Chem Res*. 2003;42(7):1478–1484.
16. Chhabra RP, Richardson JF, Non-Newtonian Flow in the Process Industries: Fundamentals and Engineering Applications, 2nd ed. Oxford: Butterworth-Heinemann, 2008.
17. Hall JF, Barigou M, Simmons MJH, Stitt EH. Mixing in unbaffled high throughput experimentation reactors. *Ind Eng Chem Res*. 2004; 43:4149–4158.
18. Alberini F, Simmons MJH, Ingram A, Stitt EH. A combined criterion to identify mixing performance for the blending of non-Newtonian fluids using a Kenics KM static mixer, 14th European Conference on Mixing, Warszawa, September 10–13, 2012, European Federation of Chemical Engineering (EFCE).
19. Brown DAR, Jones PN, Middleton JC, Papadopoulos G Arik, EB. Experimental methods. In: Paul EL, Atiemo-Obeng VA, Kresta SM, editors. Handbook of Industrial Mixing: Science and Practice. Hoboken, NJ: Wiley, 2004:145–256.

Manuscript received Nov. 5, 2012, and revision received Sept. 10, 2013.